AMERICAN JOURNAL OF PHYSIOLOGY
LUNG CELLULAR AND MOLECULAR PHYSIOLOGY

Non-uniform alveolar liquid phase thickness in alveolar edema: a conceptual analysis of the effect on oxygenation

AJPLUNG.90117.2026 | Research Article

Submitted on: 09-28-2026

Submitted by: Charul Singh,Carrie E. Perlman

Keywords: ALVEOLAR-CAPILLARY OXYGEN TRANSPORT,HARMONIC MEAN THICKNESS,ALVEOLAR LIQUID LINING LAYER,ALVEOLAR EDEMA LIQUID DISTRIBUTION,FRACTION OF INSPIRED OXYGEN

PDF auto-generated using **ReView** from RIVER VALLEY TECHNOLOGIES

Downloaded from journals.physiology.org/journal/ajplung (155.246.151.038) on October 23, 2026.

Title: Non-uniform alveolar liquid phase thickness in alveolar edema: a conceptual analysis of the effect on oxygenation

Authors
Charul Singh, Stevens Institute of Technology, Hoboken, NJ, United States
Carrie E. Perlman, Stevens Institute of Technology, Hoboken, NJ, United States

Corresponding author
Carrie E. Perlman, Ph.D.
Department of Biomedical Engineering
Stevens Institute of Technology
Hoboken, NJ 07030
cperlman@stevens.edu

Abstract
Pulmonary edema reduces lung gas exchange, but multiple mechanisms limit the reduction. We propose an additional mechanism. In flooded alveoli of excised lungs, the distribution of alveolar edema liquid is often non-uniform. Oxygen flux through a given volume of edema liquid is greater for non-uniform than uniform liquid distribution. If alveolar oxygen transport were purely diffusive, one could quantify the difference analytically using Fick's first law of diffusion. But capillary advection also influences alveolar oxygen transport. We assess alveolar oxygen transport computationally in an alveolar model generated by extruding five sides of a cube and dividing the thickness of each side into an aqueous domain (alveolar liquid and tissue, which constitute the barrier to diffusion) and a capillary blood domain. With a physiologic aqueous-domain thickness, t_B, of 0.71 µm, outlet oxygen saturation is 98%. Increasing t_B to 5 µm only reduces saturation to 97%, but increasing t_B to 15 µm reduces saturation to 85%. For the same aqueous-domain volume and interfacial area, non-uniform liquid distribution can return saturation to 89%. How non-uniform liquid distribution may interact with other mechanisms affecting oxygenation is considered. For example, alveolar edema is often accompanied by non-uniform perfusion and we find that alveolar oxygen transport drops more sharply below physiologic flow rate than it increases above. Thus non-uniform perfusion acts counter to non-uniform alveolar liquid distribution and reduces oxygenation. Our model has a functional, if simplistic, geometry; uses fundamental gas-exchange relations; and raises questions about oxygenation capability in edematous lungs.

Running title: Non-uniform alveolar edema liquid

New & Noteworthy
We find that non-uniform distribution of edema liquid within alveoli contributes to preserving gas exchange in edematous lungs.

Keywords
Alveolar-capillary oxygen transport; harmonic mean thickness; alveolar liquid lining layer; alveolar edema liquid distribution; fraction of inspired oxygen

Downloaded from journals.physiology.org/journal/ajplung (155.246.151.038) on October 23, 2026.

Introduction

Pulmonary edema reduces oxygen uptake in the lungs. It does so by thickening the aqueous domain – the combined alveolar liquid and septal tissue phases – across which oxygen must diffuse from alveolar air to capillary blood. With diffusive flux being proportional to solubility, α, (Eq. 1, below) and oxygen having a low solubility in water – 1/10 that of carbon dioxide (1) – pulmonary edema has the potential to cause a pronounced reduction in oxygen transport.

Perhaps surprisingly, experimental models of pulmonary edema have only sometimes (e.g. with hydrostatic edema or airway nebulization of acidic solution), not always (e.g. with airway nebulization of normal saline), resulted in impaired oxygenation (2,3). When oxygenation is impaired, it is despite the fact that various protective mechanisms limit the deleterious effect of edema on oxygen transport. First, with interstitial edema, liquid that leaks from the vasculature initially expands cuffs of tissue around large airways and arteries thus preserves alveolar surface area for gas exchange (4). Second, with alveolar edema, initially, discrete alveoli are flooded while others remain aerated and available for gas exchange. This pattern may be due to a surface-tension-dependent pressure barrier trapping liquid within flooded alveoli, thus may be particularly effective when surface tension is elevated in injured lungs (5,6). Third, hypoxic pulmonary vasoconstriction (HPV) and ventilatory control, via calcium signaling, of surfactant secretion promote ventilation-perfusion matching (7,8).

Here, we highlight an additional mechanism that limits the deleterious effect of pulmonary edema on oxygenation. We note that the thickness of the liquid phase within flooded alveoli, t_L, is often non-uniform (9,10) (Fig. 1). While this variability should have little effect on diffusion of highly-water-soluble carbon dioxide, it could have a significant impact on diffusion of poorly-water-soluble oxygen. The diffusive flux of oxygen across the alveolar liquid phase, J_D, is governed by Fick's first law of diffusion (1):

$$J_D = -\iint_A D\alpha\,(\Delta Po_2/t_L)dA, \quad (1)$$

where D is the diffusion coefficient for oxygen in the liquid, ΔPo_2 is the difference in the partial pressure of oxygen across the liquid phase and A is surface area. Equation 1 can be rewritten as $J_D = -D\alpha\,\Delta Po_2\,A/\bar{t}_{L/H}$, where $\bar{t}_{L/H} = A/(\iint_A 1/t_L\,dA)$ is the harmonic-mean t_L value. For a uniform-thickness liquid phase, $\bar{t}_{L/H} = t_L$. For a non-uniform-thickness liquid phase, $\bar{t}_{L/H}$ is the thickness of the equivalent uniform-thickness liquid phase through which, for a given ΔPo_2 and A, flux would be the same. Because $J_D \sim 1/t_L$, the benefit of reducing t_L in one region of an alveolus is greater than the detriment of increasing t_L in another. Thus a non-uniform liquid distribution has a lower $\bar{t}_{L/H}$, and enables greater flux, than uniform distribution of the same liquid volume (Fig. 2).

Were oxygen diffusion the only determinant of alveolar oxygen transport, one could use Eq. 1 to determine oxygen transport analytically for different intra-alveolar edema liquid distributions. But the advection of alveolar capillary blood flow also influences oxygen transport. Thus, we take a computational approach to conceptually predicting how liquid

Downloaded from journals.physiology.org/journal/ajplung (155.246.151.038) on October 23, 2026.

distribution in edematous alveoli affects oxygen transport. We assess the effects of (i) increasing thickness of a uniformly-distributed alveolar liquid phase; (ii) uniform vs. non-uniform distribution of the same edema liquid volume; (iii) varying blood flow rate and (iv) increasing fraction of inspired oxygen, F_IO_2. We perform all assessments for single alveoli and, estimating that an arteriole and venule are typically separated by ~three alveoli (11–13), select assessments across three sequential alveoli.

Materials and Methods

Geometry and domains. To predict oxygen transport in edematous alveoli, we use SOLIDWORKS (Dassault Systèmes SolidWorks Corporation, Waltham, MA) to construct the geometry of a simplified rat alveolus coated, on its surface, by pulmonary-capillary sheets (13). We model the alveolus with a cubic geometry, with five closed faces and an open top face. This approach enables simulation of an alveolus that is three-dimensional, ensuring a roughly accurate distribution of capillary path lengths; comprises planar capillary sheets, which are physiologic and enable application of symmetry boundary conditions at the mid-planes of the sheets; and facilitates assessment of comparable uniform and non-uniform liquid distributions in a way that would not be possible with a more complex geometry such as a dodecahedron.

To generate a volumetric model, we extrude five faces of a cube. Then, we divide the structure into inner and outer domains. The inner domain is a single, continuous aqueous domain that comprises (i) the alveolar liquid phase and (ii) the tissue phase (epithelium, interstitium and endothelium) that separates the alveolar liquid phase from the blood plasma in the capillary. We aggregate the tissue phase with the liquid phase because, given the low solubility of oxygen in water, the major deterrent to oxygen diffusion through tissue, whether healthy tissue or inflamed swollen tissue, is the water content of the tissue. The aqueous domain constitutes the barrier to oxygen flux from alveolar air to capillary blood and has thickness t_B. The outer domain is the capillary domain, and comprises just the blood in the septal capillaries.

We generate a model with the dimensions specified in Table 1. We use the surface area of a healthy rat-lung alveolus at a recoil pressure of 10 cmH_2O on deflation. At this pressure, healthy lungs are near total lung capacity thus somewhat more expanded than typical at peak inspiration during tidal breathing (11). For injured, ventilated lungs, 10 cmH_2O is similar to the peak recoil pressure determined from the difference between plateau pressure and end-expiratory esophageal pressure (14). But for injured lungs, as injury is spatially heterogeneous, there is not likely one appropriate surface area. Surface area of injured alveoli is likely to be reduced. Due to interdependence, aerated alveoli are likely to be overdistended (15,16). Overall, the alveolar surface area value we use should be roughly appropriate. To model only the gas exchange surface area, we further reduce the surface area to just the portion that is covered by septal capillaries (17). Under physiologic conditions, we set t_B to the typical thickness of the alveolar liquid phase over flat portions of alveolar walls, where the majority of oxygen flux occurs, plus the harmonic mean thickness of the tissue phase (18,19). To model

Downloaded from journals.physiology.org/journal/ajplung (155.246.151.038) on October 23, 2026.

injury, we increase t_B. As pulmonary capillary sheets are planar and receive diffusive oxygen flux from two alveoli, one to each side, capillary sheets are symmetric. We model the half-thickness of each capillary sheet that is adjacent to the model alveolus (20). By using the harmonic mean tissue thickness, we account for the "active" and "passive" sides of the capillaries despite modeling only half of each sheet. Finally, the capillary domain incudes an inlet and an outlet.

Meshing. To simulate blood flow and oxygen transport, we import the alveolar model geometry into COMSOL Multiphysics (COMSOL, Stockholm, Sweden). For models that are symmetrical about a mid-plane, we import half of the model and apply a symmetry boundary condition at the mid-plane. With the COMSOL default "normal" resolution, we mesh each domain using tetrahedral elements and apply corner refinement to improve mesh resolution at corners and sharp boundaries.

Blood flow. We model blood flow within the capillary domain and consider blood to be a Newtonian fluid. Blood parameters and hemodynamic boundary conditions are specified in Table 2. At the capillary-domain inlet, we specify a uniform blood velocity that results in hemoglobin saturation reaching a near-maximal value at ~1/3 of the total distance along the equatorial alveolar blood flow path (21,22) (Fig. 5C below). As inlet diameter is fixed, we effectively specify flow rate. We apply symmetry boundary conditions at the capillary mid-plane locations, i.e. at the outside (but not top) of the cubic portion of the model. At the capillary-domain outlet, we impose a pressure boundary condition. At all other capillary domain surfaces, we apply no-slip boundary conditions.

Oxygen transport. Under steady-state conditions, transport of total dissolved-plus-hemoglobin-bound oxygen through the aqueous and capillary domains can be expressed as the sum of diffusive and advective fluxes (1):

$$\nabla \cdot (-D \nabla C_D + uC_D + u K_{Hb} So_2) = 0 \quad (2)$$

where D is the diffusivity of dissolved oxygen in water or plasma, C_D is the concentration of dissolved oxygen, u is blood velocity, K_{Hb} is the oxygen-binding capacity of hemoglobin per unit blood volume and So_2 is hemoglobin saturation. The first, second and third terms describe the diffusion of dissolved oxygen, advection of dissolved oxygen and advection of hemoglobin-bound oxygen, respectively. Compared with the traditional method for assessing diffusing capacity (23), we do not consider reaction kinetics (24,25) but account for spatial variation in oxygenation.

We model the transport of dissolved oxygen – diffusive transport in the aqueous and capillary domains, advective transport in only the capillary domain – and treat hemoglobin binding of oxygen as an oxygen sink. Thus we treat the third term of Eq. 2 as a negatively-signed reaction term, R. Assuming incompressible flow:

$$R = -K_{Hb} (u \cdot \nabla So_2). \quad (3)$$

Downloaded from journals.physiology.org/journal/ajplung (155.246.151.038) on October 23, 2026.

To determine R, we express saturation as a function of the partial pressure of oxygen, Po_2, according to the Hill equation (26):

$$So_2 = \frac{P_{O2}^n}{P_{O2,50}^n + P_{O2}^n}, \quad (4)$$

where $Po_{2,50}$ is the Po_2 at which hemoglobin is 50% saturated and n is the Hill coefficient. We express Po_2, in turn, as a function of C_D according to Henry's law:

$$Po_2 = C_D/\alpha. \quad (5)$$

Finally, determining dSo_2/dPo_2 and dPo_2/dC_D from Eqs. 4 and 5, respectively, we rewrite Eq. 3 as:

$$R = -K_{Hb} \frac{dS_{O2}}{dP_{O2}} \frac{dP_{O2}}{dC_D} (u \cdot \nabla C_D). \quad (6)$$

We specify Po_2 at the boundaries of the modeled domain as follows. At the air-liquid interface of the aqueous domain – the top and pocket surfaces of the aqueous domain – we specify Po_2 as determined from F_Io_2 and the alveolar gas equation (27). At the vascular inlet, we specify Po_2 to be that of systemic venous blood. At the peripheries of the short inlet and outlet tubes and at the top surface of the capillary domain, no oxygen flux is permitted. At the capillary mid-plane locations, we apply a symmetry boundary condition for oxygen concentration that results in zero flux. All oxygen transport parameter values and boundary conditions are provided in Table 3. Oxygenation at the vascular outlet is an output of the model.

Simulations. We solve the governing equations iteratively, under steady state conditions, using the finite element method implemented in COMSOL.[1] We use a segregated approach in which, at each iteration, pressure and volume are solved for simultaneously in a first step and then oxygen concentration is solved for in a second step.

We report average values across the capillary-domain outlet of total (dissolved plus hemoglobin-bound) oxygen concentration, $\bar{C}_{T,Out}$, and of oxygen saturation, $\bar{S}o_{2,Out}$. We also calculate alveolar oxygen transport rate, $\dot{V}o_2$ as the increase in convective oxygen flux, J_C, from the inlet to the outlet of the capillary domain:

$$\text{Alveolar } \dot{V}o_2 = J_{C,Out} - J_{C,In} = \iint_{\text{Capillary-domain outlet}} uC_T dA - \iint_{\text{Capillary-domain inlet}} uC_T dA. \quad (7)$$

We simulate three types of individual alveoli: (1) a healthy alveolus with t_B = 0.71 µm (28,000/140,000 aqueous/capillary domain elements); (2) edematous alveoli with t_B thickened, uniformly, to 2, 5, 10, 15 or 20 µm (14,000-28,000/85,000 aqueous/capillary domain elements); and (3) edematous alveoli with the same alveolar liquid volume and air-liquid interfacial area as for t_B = 15 µm in (2) but with the air compartment translated toward a corner so that the liquid

[1] The COMSOL model is available online on the corresponding author's website.

Downloaded from journals.physiology.org/journal/ajplung (155.246.151.038) on October 23, 2026.

is non-uniformly distributed and, in a local region, t_B is reduced to t_{Thin} = 0.71, 2 or 5 μm (25,000-33,000/61,000-82,000 aqueous/capillary domain elements) (Fig. 3).

For a uniform t_B of 15 μm and for a corresponding non-uniform condition in which t_{Thin} = 0.71 μm, we model three alveoli in series with the Po_2 that exits one alveolus being the Po_2 that enters the next. As Po_2 varies across the capillary-domain outlet of each alveolus, we calculate the spatially-averaged value at the outlet and apply it as a constant Po_2 across the capillary-domain inlet of the next alveolus. In a slight inaccuracy, we apply the same hydrostatic pressure at the capillary domain outlet of each alveolus (Table 2). However, as the drop in absolute pressure from inlet to outlet of the capillary domain is negligible, the there is no effect on oxygenation.

Finally, for the challenging condition of uniform t_B = 15 μm, we perform parametric sweeps to assess the effects of altered flow rate in the capillary domain and altered alveolar F_Io_2.

Convergence. For all simulated conditions, numerical convergence is achieved in 16-17 iterations with relative solution error falling below a specified relative tolerance of 1 x 10^{-3}. For two scenarios, we assess solution sensitivity to mesh resolution by comparing results with the default normal resolution to those with the default fine resolution. For a healthy alveolus with t_B = 0.71 μm, the difference in $\bar{S}o_{2,Out}$ is << 0.01%. For a uniformly thickened alveolar liquid phase with t_B = 15 μm, the difference in $\bar{S}o_{2,Out}$ is 0.2%.

Results

Physiologic conditions. At the peripheries of the short inlet and outlet tubes and along the top and inner surfaces of the capillary domain, the latter being the blood-tissue phase interface, blood velocity is zero due to no-slip conditions (Fig 4A). At the mid-planes of the capillary sheets (locations of symmetry boundary conditions at outside surface of modeled capillary domain) velocity is locally maximal. And along the bottom edges of the alveolus, where the path length from inlet to outlet is longest, fluid incompressibility causes velocity to be highest. Pressure drops from inlet to outlet (Fig. 4B). The results for velocity and pressure in the capillary domain are the same for all simulations excepting those of Fig. 8A, below.

With the thin physiologic aqueous domain (t_B = 0.71 μm; Figs. 5A and 5C, top rows), total (dissolved plus hemoglobin-bound) oxygen concentration, C_T, and blood oxygen saturation, So_2, in the outer, capillary domain increase radially away from the inlet and plateau at ~1/3 the distance along the equatorial path length. The location of the So_2 plateau is specified as a part of the model design. At the capillary-domain outlet, C_T and So_2 are nearly uniform across the cross-sectional area and $\bar{S}o_{2,Out}$ equals 98%. As there is no hemoglobin in the extra-vascular aqueous domain, C_T is low in that domain and So_2 is zero.

Validation of physiologic condition. We validate the physiologic model results by extrapolating from simulated gas transport in an alveolus to that for the whole lung. According to Eqn. 7, we estimate that the $\dot{V}o_2$ in a single, healthy alveolus is 2.06 x 10^{-11} mol O_2/min.

Downloaded from journals.physiology.org/journal/ajplung (155.246.151.038) on October 23, 2026.

Given that blood from an arteriole passes over ~three alveoli before reaching a venule but blood is fully saturated by ~1/3 of the path length over the first alveolus (21,22), we multiply the single-alveolar $\dot{V}o_2$ by $N/3$, where $N = 1.97 \times 10^7$ is the total number of alveoli in a rat lung (12). We obtain an estimate for whole lung $\dot{V}o_2$ of 1.36×10^{-4} mol O_2/min, which is on the same order as the reported value of 1.67×10^{-4} mol O_2/min for a 250 g rat (28).

Effect of aqueous domain thickness on $\bar{C}_{T,Out}$ and $\bar{S}o_{2,Out}$. With a physiologic t_B of 0.71 μm, $\bar{S}o_{2,Out}$ is 98%; with t_B increased to 5 μm, $\bar{S}o_{2,Out}$ decreases only marginally to 97%. Thus, with an increase of up to ~seven-fold in t_B, $\bar{C}_{T,Out}$ and $\bar{S}o_{2,Out}$ for a single aerated alveolus remain largely preserved (Fig. 5). Beyond t_B of 5 μm, however, $\bar{C}_{T,Out}$ *and* $\bar{S}o_{2,Out}$ drop at faster, and roughly linear, rates. For this and subsequent comparisons made with fixed inlet Po_2 and vascular flow rate, $\dot{V}o_2$ will vary proportionately with $\bar{C}_{T,Out}$.

Effect of alveolar liquid distribution on $\bar{C}_{T,Out}$ and $\bar{S}o_{2,Out}$. With uniform t_B = 15 μm, C_T and So_2 increase relatively slowly from inlet to outlet (Figs 6A and 6C, top rows). The metrics increase especially slowly along the bottom edges of the alveolus where the distance from the air-liquid interface to the capillary domain is greatest (see Fig. 5A, bottom row inset). Compared with a physiologic value of 98%, $\bar{S}o_{2,Out}$ is reduced to 85% (Fig. 6D). With non-uniform distribution of the same alveolar liquid volume, unchanged air-liquid interfacial area and t_{Thin} = 0.71 μm, C_T and So_2 increase quickly in passing by the thin regions (Figs. 6A and 6C, second rows). As a result, $\bar{C}_{T,Out}$ and $\bar{S}o_{2,Out}$ (88.5%) are greater than with uniform t_B = 15 μm (Figs. 6B and 6D). As t_{Thin} increases to 2 μm and 5 μm with non-uniform distribution (Figs 6A and 6C, bottom two rows), $\bar{C}_{T,Out}$ and $\bar{S}o_{2,Out}$ (87% with t_{Thin} = 5 μm) decrease but remain greater than with uniform t_B = 15 μm.

Under physiologic conditions, modeling a single alveolus is sufficient as full saturation is reached before the alveolar capillary-domain outlet. With alveolar flooding, outlet blood is not yet saturated and modeling a single alveolus is not sufficient. As we estimate that blood from an arteriole passes over ~three alveoli before reaching a venule, we model the cases of uniform t_B = 15 μm and non-uniform distribution of the same volume with t_{Thin} = 0.71 μm for three identical alveoli arranged in series. With the same blood oxygen content at the inlet to each series of three alveoli, So_2 increases less through the first alveolus with uniform than non-uniform liquid distribution (Fig. 7). Through the second alveolus, with reduced driving ΔPo_2 in the alveolus with non-uniform liquid distribution, So_2 increases comparably in both alveoli and the difference in $\bar{S}o_{2,Out}$ remains about the same. But through the third alveolus, whether due to the yet greater reduction in ΔPo_2 in the alveolus with non-uniform liquid distribution or because So_2 in that alveolus is more closely approaching saturation, So_2 increases more in the alveolus with uniform liquid distribution and the difference in $\bar{S}o_{2,Out}$ narrows. After the third alveolus, $\bar{S}o_{2,Out}$ is 97% with uniform distribution and 98% with non-uniform distribution.

***Effect of capillary flow rate* on $\bar{C}_{T,Out}$ and alveolar $\dot{V}o_2$.** Due to HPV, vascular congestion and shunt flow, the effect of altered flow rate, which varies proportionately with velocity in our

Downloaded from journals.physiology.org/journal/ajplung (155.246.151.038) on October 23, 2026.

simulations, is of interest. As increasing velocity decreases capillary transit time, $\bar{C}_{T,Out}$ varies inversely with velocity (Fig. 8A). Further, as velocity becomes very high, convective flux within the capillary domain far exceeds diffusive flux across the aqueous domain and $\bar{C}_{T,Out}$ approaches the value of C_T at the capillary-domain inlet. The $\bar{C}_{T,Out}$ - velocity relation is nonlinear. However, even along the steeper portion of the $\bar{C}_{T,Out}$ - velocity curve at low velocity, the fractional rate at which velocity varies is greater than the fractional rate at which $\bar{C}_{T,Out}$ varies. Thus at all velocities, the effect of velocity dominates that of $\bar{C}_{T,Out}$ and alveolar $\dot{V}o_2$ varies directly with velocity (Eq. 7). That said, the reduced sensitivity of $\bar{C}_{T,Out}$ to velocity at high velocity causes the rate of change of alveolar $\dot{V}o_2$ with respect to velocity also to decrease at high velocity.

Effect of F_Io_2 on $\bar{S}o_{2,Out}$. Pulmonary edema patients are often administered an elevated F_Io_2. In the challenging case of uniform t_B = 15 μm, increasing F_Io_2 from 0.21 to 0.60 effectively increases single-alveolar $\bar{S}o_{2,Out}$ from 85% to 99% (Fig. 8B).

Discussion

Alveolar liquid phase thickness in healthy and edematous alveoli. With this modeling study, we consider how alveolar liquid phase thickness and distribution affect alveolar oxygen transport. This relation is challenging to characterize experimentally. Experimental determination of oxygen flux must be performed in fresh lungs, whether *in vivo* or *ex vivo*, but, for precision and access, alveolar structural dimensions have typically been quantified by stereology in fixed histologic sections. And fixation methods have limitations.

Rapid freezing fixes lung tissue and alveolar liquid with minimal distortion but acts only over a short spatial range. Bastacky *et al.* used this method to preserve the alveolar liquid phase in healthy rat lungs (18). Given the minimal spatial penetration of the method, they were limited to preserving the liquid layer in subpleural alveoli and additionally limited, within subpleural alveoli, to the interior of the pleural surface. Nonetheless, from Bastacky *et al.* we know that liquid distribution is non-uniform even in healthy lungs. They reported an average thickness of 0.14 μm over the flat regions of alveolar walls, greater thickness in alveolar corners and thinning over protruding septal features.

Chemical fixatives diffuse into lung tissue and liquid, penetrate more deeply and act by cross-linking molecules. Aldehyde fixatives cross-link proteins. When adjusted to physiologic osmolarity to prevent absorption/filtration and administered via the lung vasculature, aldehydes can fix the alveolar liquid phase – if it contains proteins. Under physiologic conditions, as proteins are scarce in the alveolar liquid phase, fixation is challenging (29–34); in injured lungs, protein concentration in the alveolar liquid phase is elevated and fixation is more consistently feasible. Even so, protein cross-linking can cause shrinkage, shrinkage must be minimal or uniform to maintain structural architecture and fixation technique affects the nature of the shrinkage. For the sample of Fig. 1A, Bachofen *et al.* [9] included in the fixation protocol perfusion with osmium tetroxide and uranyl acetate. Osmium tetroxide generates cross-links between double bonds, including those of unsaturated lipids such that lipid membranes are

Downloaded from journals.physiology.org/journal/ajplung (155.246.151.038) on October 23, 2026.

preserved, that are especially stable thus nearly prevent tissue shrinkage (35). Uranyl acetate dissociates; its cationic uranyl ion binds to anionic phosphate groups on phospholipids and fixes phospholipid membranes (36, 37). As a result of the extra perfusion-fixation steps, any shrinkage that occurred was uniform and the air-liquid interface remained smooth. For safety reasons, however, those steps are now omitted. As a consequence, the interfacial contour of the Fig. 1B sample is not smooth, indicating non-uniform shrinkage. This limitation notwithstanding, it is still clear in Fig. 1B that the alveolar liquid phase has non-uniform thickness.

What causes non-uniform alveolar liquid distribution in healthy and edematous alveoli? A static effect of surface tension is, most likely, the cause. Where the air-liquid interface must curve in alveolar corners, the Laplace relation dictates that liquid pressure be low; that low pressure pulls liquid toward the corners. That surface tension is sufficient to cause liquid pooling in corners is demonstrated by direct liquid injection into subpleural alveoli of excised lungs. Within seconds after injection of aqueous solution into statically-inflated lungs, we find that some liquid is retained in alveoli near the injection site and that the liquid is pooled in the alveolar corners (e.g., Fig. 2 of (5)). Following injection of low-surface-tension ethanol, in contrast, the liquid flows away from the site of injection and retention is minimal (personal observation, CEP). Dynamic ventilation and biologic function might modulate alveolar liquid distribution. With inflation during ventilation, an increase in corner interfacial curvature should further lower corner liquid pressure, draw more liquid to the corner and, along with the liquid, draw more interfacial surfactant to the corner. Consequent Marangoni forces should then pull liquid away from the corner, tending to limit additional corner pooling and maintain liquid coverage of septa even at high lung volume. (Additional dynamic effects are discussed in the *Limitations* section, below.) Corner pooling might also be limited by preferential liquid absorption in alveolar corners, where type II cells with high epithelial sodium channel expression tend to be located, or, possibly, by chloride-channel-dependent liquid secretion across type I cells that line the flat regions of alveolar walls (38,39). But, again, static surface tension effects are likely to dominate (5).

Given the discussed limitations of fixation, few data are available for the thickness of the liquid lining layer in healthy lungs. As most gas exchange occurs along the flat regions of alveolar walls, we use Bastacky *et al.'s* value of 0.14 μm for t_L in modeling healthy alveoli (18). And with use of this value, we are able to validate our physiologic results. As our results suggest that oxygenation is not sensitive to t_L until t_L exceeds ~5 μm (Fig. 5), non-uniform liquid distribution should not affect oxygenation in healthy alveoli. The lack of sensitivity of oxygenation to t_L at low t_L is interesting as we have observed t_L to be ~2-4 μm in freshly excised rat lungs in the absence of any airway/alveolar liquid instillation. We have made this observation in subpleural alveoli along septa that penetrate downward from the pleural surface toward the interior of the lungs and that separate two alveoli (40). In edematous alveoli, our modeling shows that the non-uniform distribution has an effect on oxygenation.

Downloaded from journals.physiology.org/journal/ajplung (155.246.151.038) on October 23, 2026.

Anatomic and physiologic determinants of oxygenation in heterogeneously injured lungs. The present study considers oxygenation at the alveolar level. We present novel analyses demonstrating how alveolar liquid phase thicknesses and distribution affect oxygen transport. We isolate the effect of thickness or distribution by fixing inlet Po_2 and vascular flow rate.

Across injured lungs, alveolar condition is heterogeneous with varied degrees of edema, collapse, arteriolar constriction and vascular congestion. Mathematically, if one had the appropriate data, one could calculate a flow-weighted average of $\bar{C}_{T,Out}$ values from simulations of healthy aerated alveoli; flooded alveoli with different liquid amounts/distributions and with reduced flow rates for modeling HPV-induced arteriolar constriction; aerated/flooded alveoli with reduced flow rates for modeling vascular congestion; alveoli with elevated flow rates for modeling flow rerouting away from injured alveoli/congested areas; and collapsed alveoli ($\bar{C}_{T,Out} = \bar{C}_{T,In}$). With yet greater complexity, one could account for the anatomical organization of the airways by, e.g., marginally reducing alveolar Po_2 in the >50% of alveoli located most distally along the airways (41,42). However, (i) the data are not available, which, as detailed in the next two paragraphs, is in part because the relations between different physiologic oxygenation-regulation mechanisms have not been fully characterized and (ii) as detailed in the last paragraph of this section, inlet Po_2 is not really fixed as it is, for comparison purposes, in our model.

Edematous lungs have patchy perfusion and our results provide some indication of the effect of non-uniform perfusion on oxygenation. The slope of the alveolar $\dot{V}o_2$-velocity relation decreases at high velocity/flow rate (Fig. 8A). If congestion in a region of patent alveoli caused increased flow around nearby patent alveoli, the lost oxygenation in the first region could not be fully compensated for by the increased flow in the second. Non-uniform perfusion around patent alveoli, in contrast with non-uniform liquid distribution within edematous alveoli, should have a detrimental effect on oxygenation.

It is further unknown how non-uniform alveolar liquid distribution between and within alveoli interacts with HPV, in which arterioles constrict in response, and proportionately, to alveolar-gas-side hypoxia (7). In the pulmonary circulation, arterioles and venules connect to the capillaries differently than in the systemic circulation. Multiple pulmonary arterioles feed interconnected networks of capillaries, which drain to multiple venules (43). Further, arterioles tend to be located in islands (13). This microvascular arrangement suggests that arterioles may feed into capillary beds in staggered fashion, which has implications for HPV. That is, after a first arteriole feeds a capillary bed, a second arteriole and even a third arteriole may feed into the bed before any of the flow drains to a first venule. If some alveoli were flooded, then HPV might constrict some but not all of the arterioles. And given that alveolar flooding, particularly non-uniform flooding, does not fully block oxygenation (Figs. 5-6), flooded alveoli could contribute some gas exchange to the partially-perfused capillary network. Non-uniform liquid

Downloaded from journals.physiology.org/journal/ajplung (155.246.151.038) on October 23, 2026.

distribution and HPV should be complementary in that both should tend to preserve ventilation-perfusion matching.

Under pathologic conditions, for capillary flow across a series of three alveoli, we predict $\bar{S}o_{2,Out}$ of 97 or 98% with uniform t_B = 15 μm or with non-uniform t_B/t_{Thin} = 0.71 μm, respectively (Fig. 7). Applying Eq. 7, $\dot{V}o_2$ across the sequences of three edematous alveoli equals 1.89 x 10^{-11} and 1.94 x 10^{-11} mol O_2/min for the uniform and non-uniform scenarios, respectively. These values are 91.6 and 94.2%, respectively, of healthy single-alveolar $\dot{V}o_2$. But, systemic venous Po_2 and vascular flow rate are not really fixed. Clinical data show that, in ARDS, systemic venous and arterial Po_2 values are reduced and CO is elevated (44,45). The reduction in systemic venous Po_2 and likely also the elevation in CO, with the caveat that the elevated CO should be accompanied by an increase in fractional shunt flow (46,47), should tend to increase $\dot{V}o_2$. By fixing inlet Po_2 and alveolar flow rate at the physiologic levels when modeling edematous alveoli, we likely underestimate $\dot{V}o_2$. Amidst all the factors contributing to hypoxemia in injured lungs, the particular contribution of alveolar edema would be difficult to isolate. But by modeling uniform and non-uniform distribution of a given quantity of edema liquid under the same, fixed conditions, we show that non-uniform distribution enables greater oxygen transport that uniform distribution.

Alveolar modeling limitations. Progress has been made in characterizing the morphology of the alveolar septal capillary network and the connection between septal capillaries and a venule has been captured in a cat lung (43,48,49). Still, relatively little is known about how arterioles and venules connect to the septal capillary network and how capillaries from adjacent alveoli intersect is not known (50). Thus our model of these connections is not physiologic. And the 10 μm diameter that we use at the alveolar inlet and outlet is smaller than a typical arteriole or venule. But because we effectively specify flow rate, the choice of inlet/outlet diameters has a negligible effect on oxygenation.

We model static alveoli and do not consider the effects of ventilation, thus do not consider two potentially important influences on alveolar oxygen transport. First, we do not account for the reduction, sometimes the reversal, of alveolar ventilation in injured lungs, which reduces oxygenation (51). This reduction in oxygenation is likely driven by an overall reduction in tidal volume and in turn, per the alveolar gas equation, by a reduction in P_Ao_2. Second, we omit ventilatory-motion-induced and Marangoni-induced edema-liquid vortices that are estimated to cause advective oxygen transport of the same order of magnitude as diffusive oxygen transport (52). The first omission should tend to cause our model to overestimate oxygenation whereas the second omission should tend to cause our model to underestimate oxygenation. Neither omission alters the fact that non-uniform liquid distribution should limit hypoxemia.

Because parameters are readily available, we model a rat alveolus. That said, our analysis stems from the fundamental processes of diffusion and advection. We expect that the

Downloaded from journals.physiology.org/journal/ajplung (155.246.151.038) on October 23, 2026.

trends we predict for healthy and edematous rat alveoli would be similar for healthy and edematous human alveoli.

Conclusions. We present non-uniform alveolar edema liquid distribution as a pathophysiologic phenomenon that could contribute to preserving gas exchange in edematous lungs. It is one of multiple mechanisms acting to improve, or to reduce, oxygenation in edematous lungs. The determinants of net oxygen uptake in edematous lungs are complex and have yet to be fully characterized. This analysis serves to identify alveolar-scale trends in oxygenation in the presence of edema and to raise questions about interactions with larger-scale pulmonary and systemic influences on oxygenation.

Acknowledgements

We thank Dr. Tsengming Chou for granting access to the Stevens Institute of Technology Laboratory for Multiscale Imaging computing resources, on which we performed the simulations for this study. And we thank Dr. Matthias Ochs for his discussion of perfusion fixation techniques.

Grant

This study was funded by NIH grant R56 HL113577 (CEP).

Disclosures

The authors have no conflicts of interest to disclose.

Author contributions

This study was conceived of by CS and CEP and performed by CS. The manuscript was written and edited by CS and CEP.

Downloaded from journals.physiology.org/journal/ajplung (155.246.151.038) on October 23, 2026.

References:

1. 1. Cussler EL. Diffusion: Mass Transfer in Fluid Systems. Cambridge University Press,2009.

2. Slama K, Gesch M, Böck JC, Pietschmann SM, Schaffartzik W, Pison U. Unilateral lung edema: Effects on pulmonary gas exchange, hemodynamics, and pulmonary perfusion distribution. J Appl Physiol 89:1513–21, 2000. doi:10.1152/jappl.2000.89.4.1513

3. Said SI, Longacher JW. Pulmonary gas exchange during induction of pulmonary edema in anesthetized dogs. J Appl Physiol 19:403–7, 1964. doi:10.1152/jappl.1964.19.3.403

4. Staub NC, Nagano H, Pearce ML. Pulmonary edema in dogs, especially the sequence of fluid accumulation in lungs. J Appl Physiol 22:227–40, 1967. doi:10.1152/jappl.1967.22.2.227

5. Wu Y, Nguyen TL, Perlman CE. Accelerated deflation promotes homogeneous airspace liquid distribution in the edematous lung. J Appl Physiol 122:739–51, 2017. doi:10.1152/japplphysiol.00526.2016

6. Nguyen TL, Perlman CE. Sulforhodamine B and exogenous surfactant effects on alveolar surface tension under acute respiratory distress syndrome conditions. J Appl Physiol 129:1505–13, 2020. doi:10.1152/japplphysiol.00422.2020

7. Marshall C, Marshall B. Site and sensitivity for stimulation of hypoxic pulmonary vasoconstriction. J Appl Physiol 55:711–6, 1983. doi:10.1152/jappl.1983.55.3.711

8. Kiefmann M, Tank S, Tritt MO, Keller P, Heckel K, Schulte-Uentrop L, et al. Dead space ventilation promotes alveolar hypocapnia reducing surfactant secretion by altering mitochondrial function. Thorax 74:219–28, 2019. doi:10.1136/thoraxjnl-2018-211864

9. Bachofen H, Schürch S, Michel RP, Weibel ER. Experimental hydrostatic pulmonary edema in rabbit lungs: Morphology. Am Rev Respir Dis 147:989–96, 1993. doi:10.1164/ajrccm/147.4.989

10. Fehrenbach A, Fehrenbach H, Wittwer T, Ochs M, Wahlers T, Richter J. Evaluation of pulmonary edema: Stereological versus gravimetrical analysis. Eur Surg Res 33:270–8, 2001. doi:10.1159/000049717

11. Mercer RR, Laco JM, Crapo JD. Three-dimensional reconstruction of alveoli in the rat lung for pressure-volume relationships. J Appl Physiol 62:1480–7, 1987. doi:10.1152/jappl.1987.62.4.1480

12. Mercer RR, Russell ML, Crapo JD. Alveolar septal structure in different species. J Appl Physiol 77:1060–6, 1994. doi:10.1152/jappl.1994.77.3.1060

13. Sobin SS, Fung YC, Lindal RG, Tremer HM, Clark L. Topology of pulmonary arterioles, capillaries, and venules in the cat. Microvasc Res 19:217–33, 1980. doi:10.1016/0026-2862(80)90042-4

14. Beitler JR, Sarge T, Banner-Goodspeed VM, Gong MN, Cook D, Novack V, et al. Effect of titrating positive end-expiratory pressure (PEEP) with an esophageal pressure–guided strategy vs an empirical High PEEP-F_{IO_2} strategy on death and days free from mechanical ventilation among

Downloaded from journals.physiology.org/journal/ajplung (155.246.151.038) on October 23, 2026.

patients with acute respiratory distress syndrome: A randomized clinical trial. JAMA 21:846-57, 2019. doi:10.1001/jama.2019.0555

15. Mead J, Takishima T, Leith D. Stress distribution in lungs: A model of pulmonary elasticity. J Appl Physiol 28:596–608, 1970. doi:10.1152/jappl.1970.28.5.596

16. Perlman CE, Lederer DJ, Bhattacharya J. Micromechanics of alveolar edema. Am J Respir Cell Mol Biol 44:34–9, 2011. doi:10.1165/rcmb.2009-0005OC

17. Fung YC, Sobin SS. Theory of sheet flow in lung alveoli. J Appl Physiol 26:472–88, 1969. doi:10.1152/jappl.1969.26.4.472

18. Bastacky J, Lee CY, Goerke J, Koushafar H, Yager D, Kenaga L, et al. Alveolar lining layer is thin and continuous: Low-temperature scanning electron microscopy of rat lung. J Appl Physiol 79:1615–28, 1995. doi:10.1152/jappl.1995.79.5.1615

19. Weibel ER, Knight BW. A morphometric study on the thickness of the pulmonary air-blood barrier. J Cell Bio 21:367–84, 1964. doi:10.1083/jcb.21.3.367

20. Short AC, Montoya ML, Gebb SA, Presson RG, Wagner WW, Capen RL. Pulmonary capillary diameters and recruitment characteristics in subpleural and interior networks. J Appl Physiol 80(5):1568–73, 1996. doi:10.1152/jappl.1996.80.5.1568

21. Pittman RN. Regulation of Tissue Oxygenation [Online]. Morgan & Claypool Life Sciences, 2011. http://www.ncbi.nlm.nih.gov/books/NBK54104/ [2026 Jan 12]

22. Si XA, Xi J. Pulmonary oxygen exchange in a rhythmically expanding–contracting alveolus–capillary model. J Respir 2:159–73, 2022. doi:10.3390/jor2040015

23. Hegewald MJ. Diffusing capacity. Clinic Rev Allerg Immunol 37:159–66, 2009. doi:10.1007/s12016-009-8125-2

24. Ilgenfritz G, Schuster TM. Kinetics of oxygen binding to human hemoglobin. J Biol Chem 249:2959–73, 1974. doi:10.1016/S0021-9258(19)42725-7

25. Whiteley JP, Gavaghan DJ, Hahn CEW. Some factors affecting oxygen uptake by red blood cells in the pulmonary capillaries. Math Biosci 169:153–72, 2001. doi:10.1016/S0025-5564(00)00060-2

26. O'Riordan JF, Goldstick TK, Ditzel J, Ernest JT. Characterization of oxygen-hemoglobin equilibrium curves using nonlinear regression of the hill equation: Parameter values for normal human adults. Adv Exp Med Biol 159:435–44, 1983. doi:10.1007/978-1-4684-7790-0_37

27. Curran-Everett D. A classic learning opportunity from Fenn, Rahn, and Otis (1946): The alveolar gas equation. Adv Physiol Educ 30:58–62, 2006. doi:10.1152/advan.00076.2005

28. Altman PL, Dittmer DS. Respiration and Circulation. Federation of American Societies for Experimental Biology, 1971.

Downloaded from journals.physiology.org/journal/ajplung (155.246.151.038) on October 23, 2026.

29. Boston RW, Humphreys PW, Normand ICS, Reynolds EO, Strang LB. Formation of liquid in the lungs of the foetal Lamb. Biol Neonat 12:306–15, 1968. doi:10.1159/000240117

30. Reifenrath R, Zimmermann I. Blood plasma contamination of the lung alveolar surfactant obtained by various sampling techniques. Respir Physiol 18:238–48, 1973. doi:10.1016/0034-5687(73)90053-4

31. Reifenrath R. Chemical analysis of the lung alveolar surfactant obtained by alveolar micropuncture. Respir Physiol 19:35–46, 1973. doi:10.1016/0034-5687(73)90088-1

32. Kikkawa Y. Morphology of alveolar lining layer. Anat Rec 167:389–400. 1970. doi:10.1002/ar.1091670403

33. Weibel ER, Gil J. Electron microscopic demonstration of an extracellular duplex lining layer of alveoli. Respir Physiol 4:42–57, 1968. doi:10.1016/0034-5687(68)90006-6

34. Rühl N, Lopez-Rodriguez E, Albert K, Smith BJ, Weaver TE, Ochs M, et al. Surfactant protein B deficiency induced high surface tension: Relationship between alveolar micromechanics, alveolar fluid properties and alveolar epithelial cell injury. Int J Mol Sci 20:4243, 2019. doi:10.3390/ijms20174243

35. Litman R. The Mechanism of the Fixation of Tissue Components by Osmium Tetroxide [Online]. Yale Medicine Thesis Digital Library, 1970. https://elischolar.library.yale.edu/ymtdl/3557 [2026 Sept 8]

36. Huang TH, Blume A, Das Gupta SK, Griffin RG. Nuclear magnetic resonance and calorimetric study of the structure, dynamics, and phase behavior of uranyl ion/dipalmitoylphosphatidylcholine complexes. Biophys J 54:173–9, 1988. doi:10.1016/S0006-3495(88)82942-4

37. Silva MT, Carvalho Guerra F, Magalhães MM. The fixative action of uranyl acetate in electron microscopy. Experientia 24:1074, 1968. doi:10.1007/BF02138757

38. Talbot CL, Bosworth DG, Briley EL, Fenstermacher DA, Boucher RC, Gabriel SE, et al. Quantitation and localization of ENaC subunit expression in fetal, newborn, and adult mouse lung. Am J Respir Cell and Mol Biol 20:398–406, 1999. doi:10.1165/ajrcmb.20.3.3283

39. Lindert J, Perlman CE, Parthasarathi K, Bhattacharya J. Chloride-dependent secretion of alveolar wall liquid determined by optical-sectioning microscopy. Am J Respir Cell Mol Biol 36:688–96, 2007. doi:10.1165/rcmb.2006-0347OC

40. Wu (吴右) Y, Kharge AB, Perlman CE. Lung ventilation injures areas with discrete alveolar flooding, in a surface tension-dependent fashion. J Appl Physiol 117:788–96, 2014. doi:10.1152/japplphysiol.00569.2014

41. Weibel ER. Modeling structure-function interdependence of pulmonary gas exchange. Adv Exp Med Biol 605:195-200, 2008. doi: 10.1007/978-0-387-73693-8_34

42. Shelley DA, Sih BL, Ng LJ. An integrated physiology model to study regional lung damage effects and the physiologic response. Theor Biol Med Model 11:32, 2014. doi:10.1186/1742-4682-11-32

Downloaded from journals.physiology.org/journal/ajplung (155.246.151.038) on October 23, 2026.

43. Buchacker T, Mühlfeld C, Wrede C, Wagner WL, Beare R, McCormick M, et al. Assessment of the alveolar capillary network in the postnatal mouse lung in 3D using serial block-face scanning electron microscopy. Front Physiol 10:1357, 2019. doi:10.3389/fphys.2019.01357

44. Czer LSC, Appel P, Shoemaker WC. Pathogenesis of respiratory failure (ARDS) after hemorrhage and trauma: II. Cardiorespiratory patterns after development of ARDS. Crit Care Med 8:513–8, 1980. doi:10.1097/00003246-198009000-00007

45. Laghi F, Siegel JH, Rivkind AI, Chiarla C, DeGaetano A, Blevins S, et al. Respiratory index/pulmonary shunt relationship: Quantification of severity and prognosis in the post-traumatic adult respiratory distress syndrome. Crit Care Med 17:1121–8, 1989.

46. Dantzker DR, Lynch JP, Weg JG. Depression of cardiac output is a mechanism of shunt reduction in the therapy of acute respiratory failure. Chest 77:636–42, 1980. doi:10.1378/chest.77.5.636

47. Granger WM, Miller DA, Ehrhart IC, Hofman WF. The effect of blood flow and diffusion impairment on pulmonary gas exchange: A computer model. Comput Biomed Res 20:497–506, 1987. doi:10.1016/0010-4809(87)90037-1

48. Grothausmann R, Knudsen L, Ochs M, Mühlfeld C. Digital 3D reconstructions using histological serial sections of lung tissue including the alveolar capillary network. Am J Physiol Lung Cell Mol Physiol 312:L243–57, 2017. doi:10.1152/ajplung.00326.2016

49. Fung, YC. Biomechanics: Circulation. Springer, 1996.

50. Schmid K, Olivares AL, Camara O, Kuebler WM, Ochs M, Hocke AC, et al. Inference of alveolar capillary network connectivity from blood flow dynamics. Am J Physiol Lung Cell Mol Physiol 327:L852–66, 2024. doi:10.1152/ajplung.00025.2024

51. Tabuchi A, Nickles HT, Kim M, Semple JW, Koch E, Brochard L, et al. Acute lung injury causes asynchronous alveolar ventilation that can be corrected by individual sighs. Am J Respir Crit Care Med 193:396–406, 2016. doi:10.1164/rccm.201505-0901OC

52. Wei HH, Fujioka H, Hirschl RB, Grotberg JB. A model of flow and surfactant transport in an oscillatory alveolus partially filled with liquid. Phys Fluids 17:031510, 2005. doi:10.1063/1.1830487

53. Lillie LE, Temple NJ, Florence LZ. Reference values for young normal Sprague-Dawley rats: Weight gain, hematology and clinical chemistry. Hum Exp Toxicol 15:612–6, 1996. doi:10.1177/096032719601500802

54. Guyton AC, Hall JE. Textbook of Medical Physiology. W.B. Saunders Company, 1996.

55. Gaehtgens, P. Flow of blood through narrow capillaries: Rheological mechanisms determining capillary hematocrit and apparent viscosity1. Biorheology 17:183–9, 1980. https://doi.org/10.3233/BIR-1980-171-220.

56. Barbee JH. The effect of temperature on the relative viscosity of human blood. Biorheology 10:1–5, 1973. doi: 10.3233/bir-1973-10101

Downloaded from journals.physiology.org/journal/ajplung (155.246.151.038) on October 23, 2026.

57. Noresson E, Ricksten S, Thorén P. Left atrial pressure in normotensive and spontaneously hypertensive rats. Acta Physiol Scand 107:9–12, 1979. doi:10.1111/j.1748-1716.1979.tb06436.x

58. Hillyard R, Anderson J, Raj JU. Segmental vascular resistance in isolated perfused rat lungs. Influence of vasomotor tone and cyclooxygenase and lipoxygenase inhibition. Circ Res 68:1020–6, 1991. doi:10.1161/01.RES.68.4.1020

59. Han P, Bartels DM. Temperature dependence of oxygen diffusion in H_2O and D_2O. J Phys Chem 100:5597–602, 1996. doi:10.1021/jp952903y

60. Christmas KM, Bassingthwaighte JB. Equations for O_2 and CO_2 solubilities in saline and plasma: Combining temperature and density dependences. J Appl Physiol 122:1313–20, 2017. doi:10.1152/japplphysiol.01124.2016

61. Fournier RL. Basic Transport Phenomena in Biomedical Engineering. CRC Press, 2017

Downloaded from journals.physiology.org/journal/ajplung (155.246.151.038) on October 23, 2026.

Figure legends:

Figure 1. **Alveolar edema liquid distribution.** Light micrographs of edematous alveoli in perfusion-fixed lungs. Edema liquid distribution is variable with thick (red arrows) and thin (cyan arrows) regions. Scale bar lengths are 20 mm. Images are modified, with permission, from Bachofen *et al.* [9] (left) and Fehrenbach *et al.* [10] (right).

Figure 2. Effect of liquid layer uniformity on harmonic mean thickness. A. Uniform liquid layer with thickness t_L = 1 and arbitrary uniform depth into page. Harmonic mean thicknesses is $\bar{t}_{L/H}$ = t_L. **B.** Non-uniform liquid layer with same volume as (A); $\bar{t}_{L/H}$ = 0.91.

Figure 3. Alveolar geometries used to model oxygen transport under healthy and edematous conditions. Capillary domains are red, aqueous domains (see text) are blue and air domains are transparent, depressed regions. Left and middle columns show different views of same alveoli; white dots label same vertex in all views, in this and subsequent figures. White arrows show direction of flow at capillary domain inlet and outlet, in this and subsequent figures. Right column shows top views. **A.** Healthy alveolus with uniform aqueous domain barrier thickness, t_B, of 0.71 μm along side and bottom surfaces. **B.** Edematous alveolus with uniform t_B of 15 μm along side and bottom surfaces. **C.** Edematous alveolus with same aqueous domain volume and air-aqueous domain interfacial area as in (B) but air domain translated toward back left corner such that aqueous domain has non-uniform distribution. In this configuration, t_B in the thin regions is t_{Thin} = 0.71 μm. Along bottom surface, t_B remains 15 μm.

Figure 4. Capillary domain velocity and pressure. A. Blood flow velocity in capillary domain. Across inlet, velocity is specified as spatially uniform. Across outlet, average velocity is same as at inlet but velocity varies with radial position. White dashed lines indicate interior edges of capillary domain. **B.** Blood pressure in capillary domain.

Figure 5. Effect of uniformly-increased thickness of aqueous domain on oxygenation. Aqueous domain constitutes barrier to diffusion between alveolar air and capillary blood, and has thickness t_B. **A.** Total (dissolved plus hemoglobin-bound) oxygen concentration in capillary and aqueous domains. Concentration is lower in aqueous than capillary domain due to lack of hemoglobin. White dashed lines indicate interior edges of aqueous domain. Yellow dashed line marks equatorial blood flow path; yellow arrowhead indicates location, at about ~1/3 of path length, at which oxygenation is near-maximal. Inset below last row shows that aqueous domain thickness is uniform along all walls. Dashed yellow line on inset shows that capillary path length along bottom edges of alveolus is furthest from air-liquid interface. **B.** Average total oxygen concentration at capillary domain outlet, $\bar{C}_{T,Out}$, as function of t_B. **C.** Oxygen saturation in capillary domain. Aqueous domain is transparent as it contains no hemoglobin. Capillary domain inlets, obscured by dark blue coloration, are highlighted by white dashed circles in this and next figure. **D.** Average oxygen saturation at capillary domain outlet, $\bar{S}o_{2,Out}$, as function of t_B.

Downloaded from journals.physiology.org/journal/ajplung (155.246.151.038) on October 23, 2026.

Figure 6. Effect of uniformity of t_B on oxygenation. A. Total oxygen concentration with uniform aqueous phase distribution and with the same aqueous phase volume and same air-aqueous phase interfacial area but different, non-uniform aqueous phase distributions. **B.** $\bar{C}_{T,Out}$ for different aqueous phase liquid distributions. **C.** Oxygen saturation in capillary domain. **D.** $\bar{S}o_{2,Out}$ for different aqueous phase liquid distributions.

Figure 7. Oxygenation with blood flow across three sequential alveoli. For blood flow across three sequential edematous alveoli with uniform aqueous domain liquid thickness t_B = 15 µm or non-uniform distribution and t_{Thin} = 0.71 µm, $\bar{S}o_{2,Out}$ at the outlet of each alveolus. Saturation contour plots are for third alveoli.

Figure 8. Parametric sweeps for flow rate and alveolar oxygenation. Results are for single alveolus with uniform aqueous-domain liquid thickness t_B = 15 µm. **A.** $\bar{C}_{T,Out}$ (gray) and net alveolar oxygen transport, $\dot{V}o_2$, (black) as functions of inlet velocity. As inlet has fixed area, results show effect of flow rate. Blue arrow indicates velocity used in all other simulations. **B.** $\bar{S}o_{2,Out}$ as a function of fraction of inspired oxygen, F_Io_2.

Downloaded from journals.physiology.org/journal/ajplung (155.246.151.038) on October 23, 2026.

Table 1. Alveolar model dimensions. All data are obtained from investigations in rats.

Parameter	Value	Explanation
Alveolar surface area	13,433 μm^2	At 10 cmH_2O recoil pressure, on deflation, rat alveolar surface area is 14,762 μm^2 (11). Estimating the fractional area covered by capillaries to be equal to the solidity ratio – the ratio of the volume occupied by blood to the total volume of the alveolar sheet – which is 0.91 (17), surface area is reduced by 9%.
Model alveolar cube side length	52 μm	Side length of cube for which summed surface area of five faces is 13,433 μm^2.
Alveolar liquid-phase thickness	0.14 μm	Typical alveolar liquid phase thickness over flat portions of alveolar walls (18).
Tissue phase (combined epithelium, interstitium, endothelium) thickness	0.57 μm	Harmonic mean thickness of tissue phase (19).
Total aqueous domain thickness	0.71 μm	Sum of alveolar liquid-phase and tissue phase thicknesses.
Capillary-domain thickness	2.5 μm	As model comprises half of capillary sheet thicknesses, with symmetry boundary conditions applied at capillary sheet mid-planes, value is half of rat capillary diameter of 5.15 μm (20).
Vascular inlet and outlet diameters	10 μm	Chosen arbitrary, as physiologic morphology is not known and parameter does not affect oxygenation.

Downloaded from journals.physiology.org/journal/ajplung (155.246.151.038) on October 23, 2026.

Table 2: Blood parameters and hemodynamic capillary-domain boundary conditions.

Parameter	Value	Explanation
Maximum oxygen binding capacity of hemoglobin, per unit volume of blood	8.69 μmol/ml	Product of the hemoglobin, Hb, concentration in blood (14 g Hb/dL) and the maximum quantity of oxygen that can be carried per gram of hemoglobin (1.39 mL O_2/g Hb or 6.2 x 10^{-5} mol O_2/g Hb) (53,54).
Blood density	1.055 g/ml	Using a hematocrit, HCT, of 0.35 (normal HCT of 0.45 adjusted according to Fahraeus effect for conduit with diameter of capillary), estimate blood density as HCT-weighted average of plasma density (1.035 g/ml at 37 °C) and red blood cell density (1.090 g/ml at 37 °C) (28,55).
Blood viscosity	1.1 cP	In large vessels at 37 °C, plasma viscosity is 1.25 cP and whole blood viscosity is 2.5 times greater, or 3.13 cP (28,56). Due to Fahraeus-Lindqvist effect, blood viscosity in a 5.15 μm diameter capillary is reduced to 35% of large-vessel blood viscosity (55).
Alveolar capillary-domain inlet blood velocity	2.12 mm/s	Set so that, under physiologic conditions, the oxygen saturation of hemoglobin approaches its maximum value at ~1/3 the capillary path length around the alveolus (21,22).
Alveolar capillary-domain outlet pressure	7.55 cmH_2O	Estimated as end-expiratory left atrial pressure in rats (6.25 cmH_2O (57)) plus the pulmonary venule-left atrial pressure difference in rats (1.3 cmH_2O (58)).

Downloaded from journals.physiology.org/journal/ajplung (155.246.151.038) on October 23, 2026.

Table 3: Oxygenation parameters and boundary conditions. Abbreviations: *D* – diffusion coefficient at 37 °C, α – solubility at 37 °C, *n* – Hill coefficient, Po_2 – partial pressure of oxygen, $Po_{2,50}$ – Po_2 at which hemoglobin is 50% saturated.

Parameter	Value, units	Citation/explanation
D for oxygen in water	3.3×10^{-5} cm^2/s	(28,59)
α for oxygen in water	1.4×10^{-6} (mol O_2/L)/mmHg plasma	(28)
D for oxygen in plasma	1.9×10^{-5} cm^2/s	(28)
α for oxygen in plasma	1.2×10^{-6} (mol O_2/L)/mmHg plasma	(28,60)
n	2.7	(61)
$Po_{2,50}$	26 mmHg	(61)
Air-aqueous domain interfacial Po_2	Varies with F_IO_2, 100 mmHg for 0.21 F_IO_2	Calculated according to alveolar gas equation (27).
Capillary-domain inlet Po_2	40 mmHg	Po_2 of systemic venous blood.

Downloaded from journals.physiology.org/journal/ajplung (155.246.151.038) on October 23, 2026.

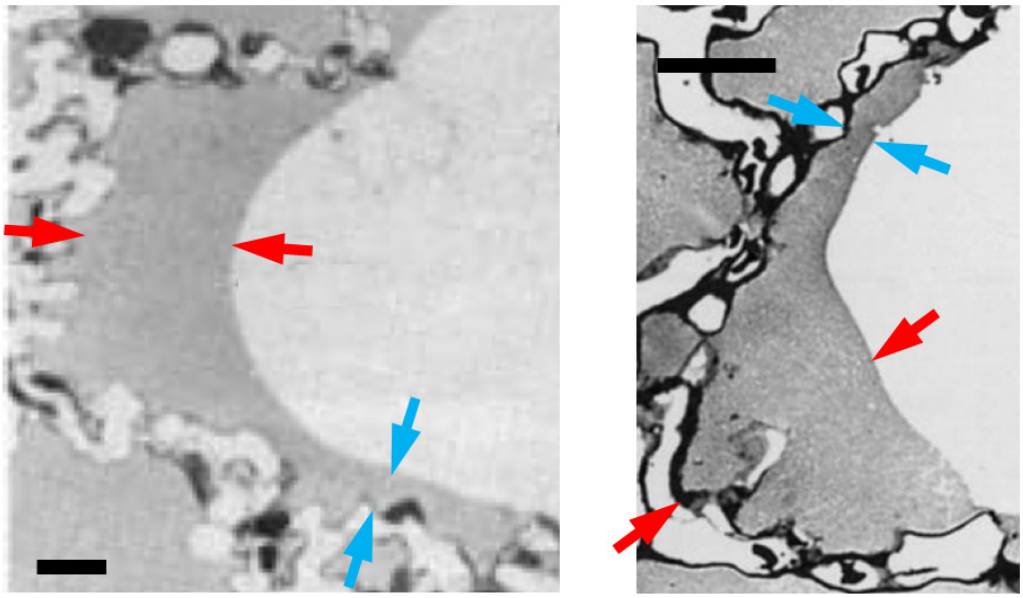


Figure 1

Downloaded from journals.physiology.org/journal/ajplung (155.246.151.038) on October 23, 2026.

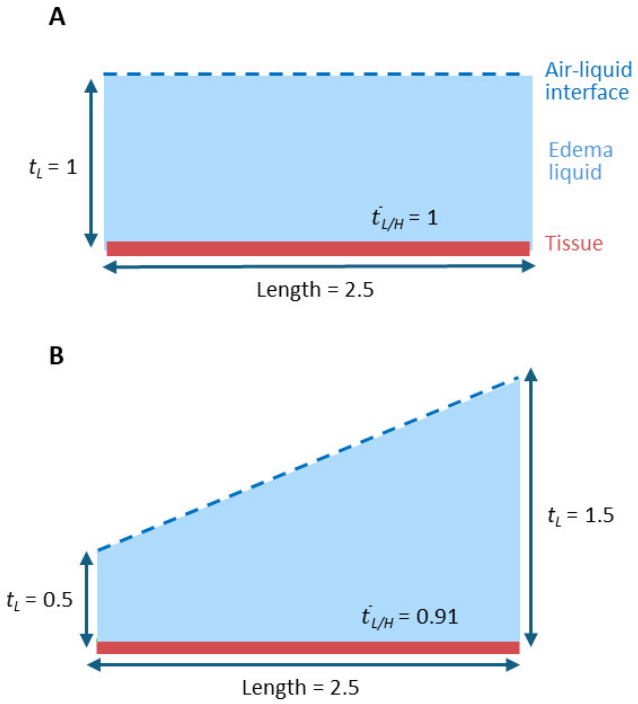


Figure 2

Downloaded from journals.physiology.org/journal/ajplung (155.246.151.038) on October 23, 2026.

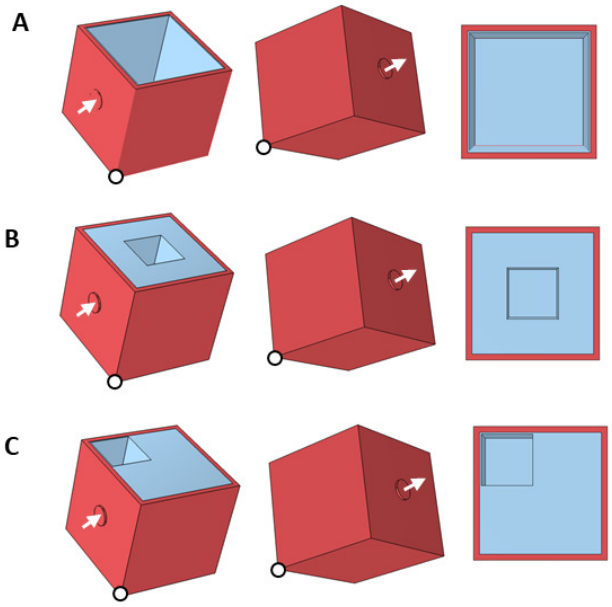


Figure 3

Downloaded from journals.physiology.org/journal/ajplung (155.246.151.038) on October 23, 2026.

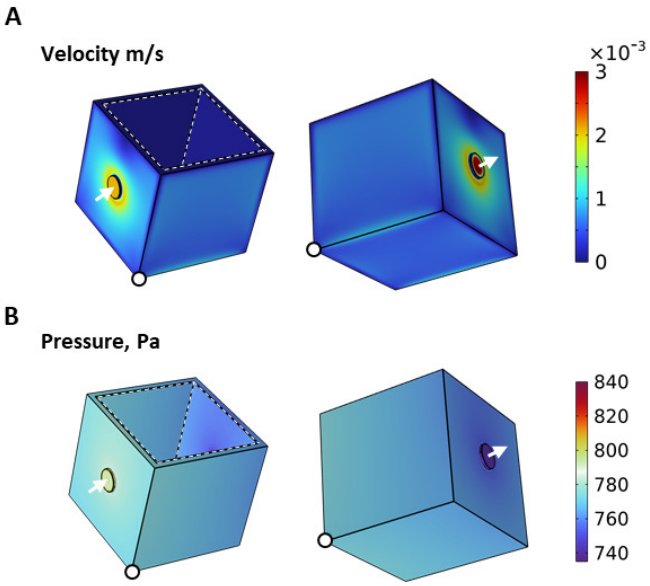


Figure 4

Downloaded from journals.physiology.org/journal/ajplung (155.246.151.038) on October 23, 2026.

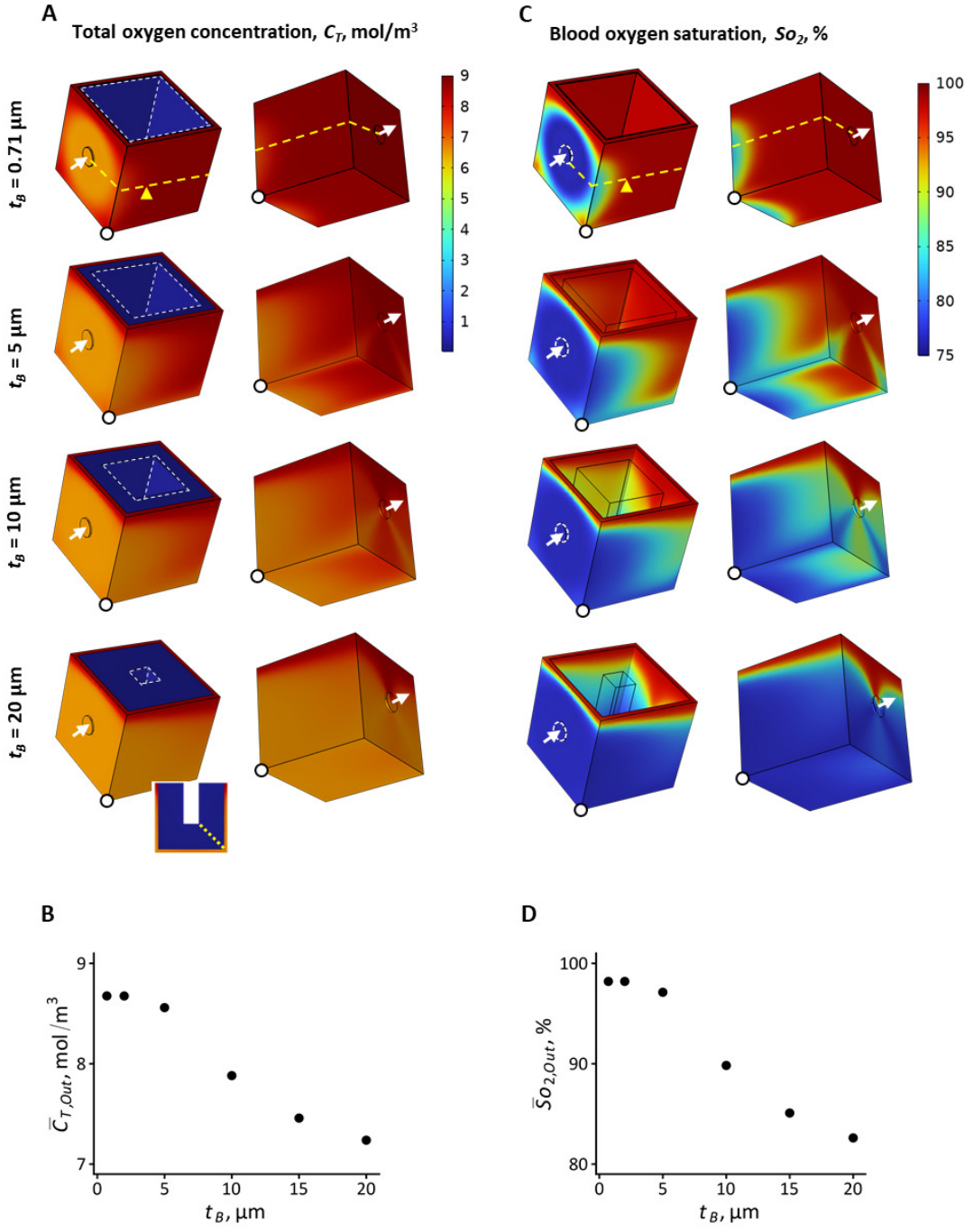


Figure 5

Downloaded from journals.physiology.org/journal/ajplung (155.246.151.038) on October 23, 2026.

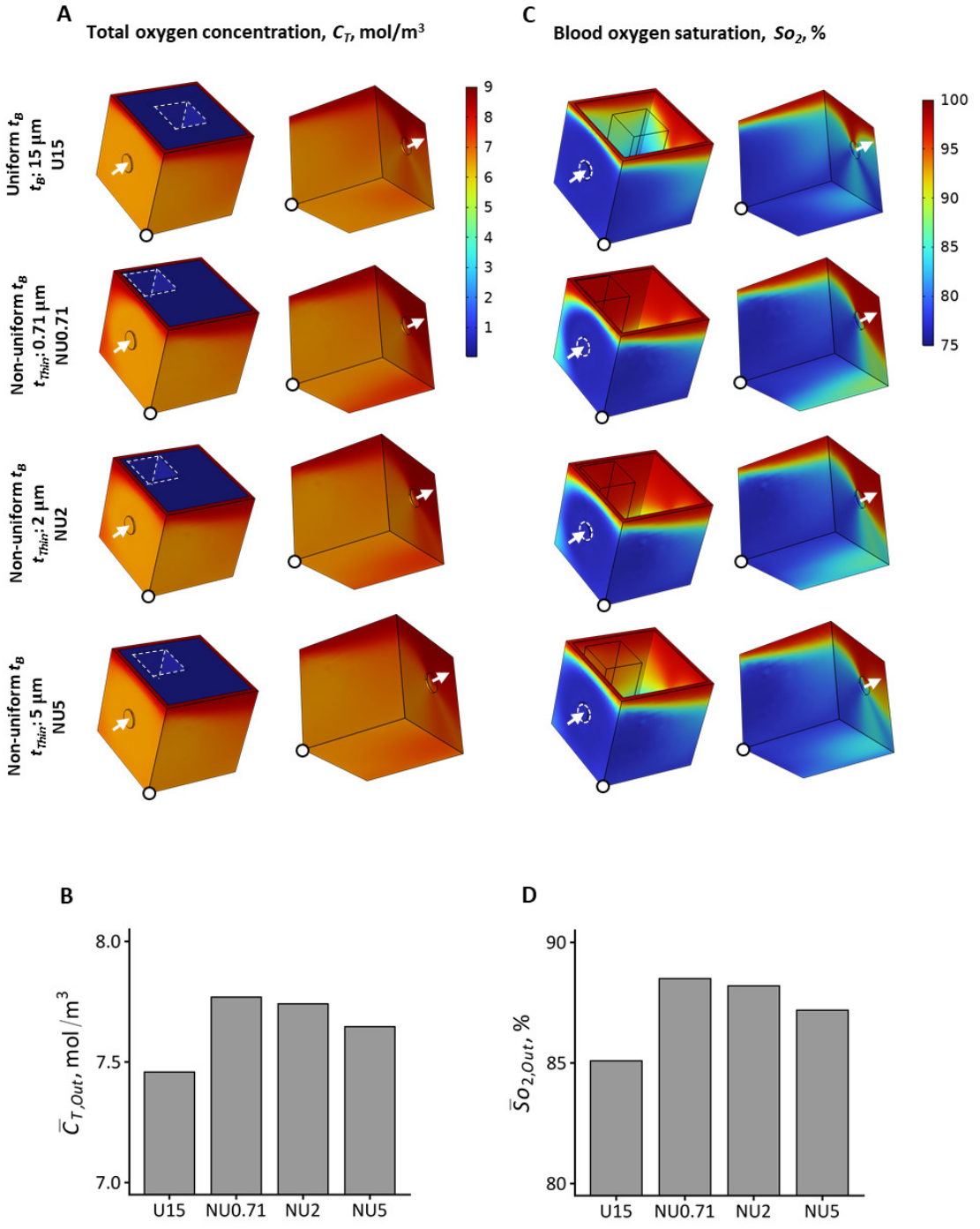


Figure 6

Downloaded from journals.physiology.org/journal/ajplung (155.246.151.038) on October 23, 2026.

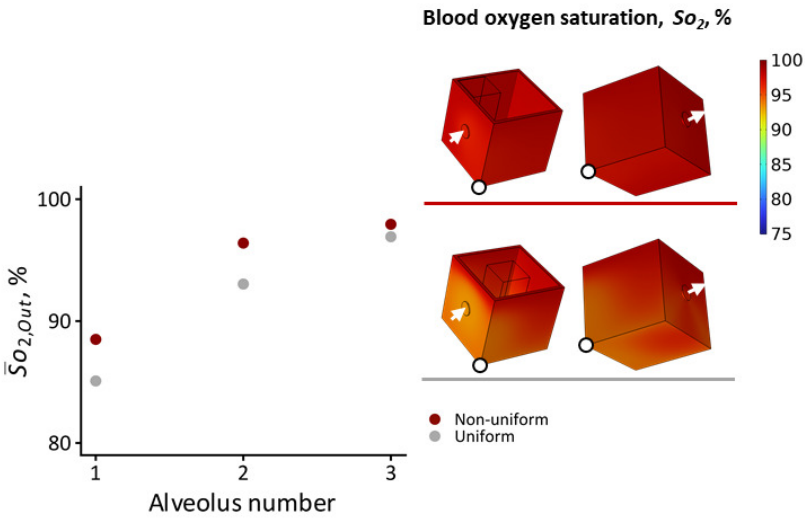


Figure 7

Downloaded from journals.physiology.org/journal/ajplung (155.246.151.038) on October 23, 2026.

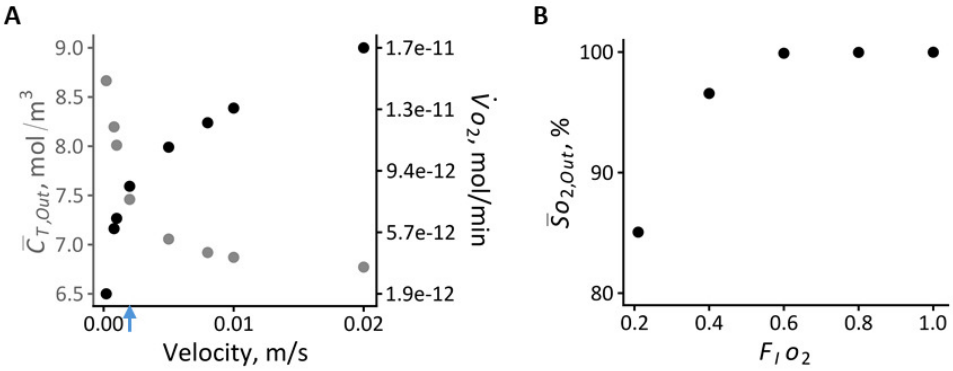
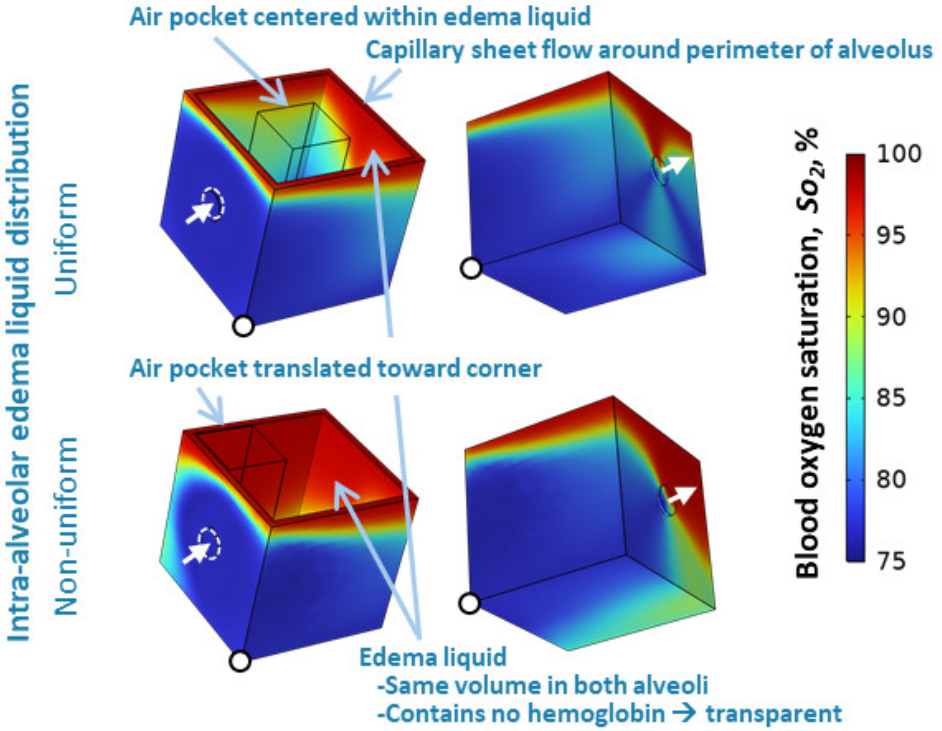


Figure 8

Downloaded from journals.physiology.org/journal/ajplung (155.246.151.038) on October 23, 2026.

Rationale: Edema liquid tends to be distributed non-uniformly within alveoli
Question: Does non-uniform edema liquid distribution improve oxygenation?
Method: Computational modeling study



Result:
Non-uniform alveolar edema liquid distribution improves oxygenation

Downloaded from journals.physiology.org/journal/ajplung (155.246.151.038) on October 23, 2026.